Three-Dimensional Models of Topological Insulators: Engineering of Dirac Cones and Robustness of the Spin Texture

David Soriano,[1] Frank Ortmann,[1] and Stephan Roche[1,2]

[1]*CIN2 (ICN-CSIC) and Universitat Autònoma de Barcelona, Catalan Institute of Nanotechnology, Campus de la UAB, 08193 Bellaterra (Barcelona), Spain*

[2]*ICREA, Institució Catalana de Recerca i Estudis Avançats, 08010 Barcelona, Spain*

(Received 11 June 2012; published 26 December 2012)

We design three-dimensional models of topological insulator thin films, showing a tunability of the odd number of Dirac cones driven by the atomic-scale geometry at the boundaries. A single Dirac cone at the Γ-point can be obtained as well as full suppression of quantum tunneling between Dirac states at geometrically differentiated surfaces. The spin texture of surface states changes from a spin-momentum-locking symmetry to a surface spin randomization upon the introduction of bulk disorder. These findings illustrate the richness of the Dirac physics emerging in thin films of topological insulators and may prove utile for engineering Dirac cones and for quantifying bulk disorder in materials with ultraclean surfaces.

DOI: 10.1103/PhysRevLett.109.266805 PACS numbers: 73.20.At, 71.23.−k, 71.70.Ej

The nascent field of topological insulators (TI) sparked by the seminal paper of Kane and Mele [1], together with the prediction of three-dimensional structures for TI [2], and the subsequent experimental discoveries of two-dimensional HgCdTe quantum wells [3] and three-dimensional TI (3D-TI) materials [4–8] has thrust these fascinating materials to the forefront of modern condensed matter physics [9–11]. Topological insulators are governed by strong spin-orbit coupling and special crystalline symmetries that yield an insulating bulk phase complemented by highly robust, gapless Dirac boundary states, revealed through spin-resolved angle-resolved photoemission spectroscopy profiles or through peculiar Landau level fingerprints in scanning tunneling spectroscopy measurements [12–14]. However, despite the success in identifying these chiral surface states by photoemission and scanning tunneling spectroscopy, the nature of surface transport in 3D-TI lacks experimental characterization. This is because, in all the materials studied to date, residual conduction through bulk states is irremediably driven by unintentional doping introduced by impurities, electrical gates or contacts [15,16].

The aforementioned boundary states are described by Dirac-cone physics, similarly to the case of low-energy excitations in graphene [17], but with Dirac cones appearing in odd numbers. The robustness of the physics of these chiral states, with respect to the thickness of a TI film, deserves particular attention. Indeed when TI are reduced to thin films, quantum tunneling between Dirac states at opposite surfaces can eventually occur, yielding gap formation, as recently shown for Bi_2Se_3 [18] or freestanding thin Sb films [19]. However, surprisingly, specific interactions between the film and substrate prevent gap formation [19], a feature which could be of considerable interest for spintronic applications but which remains poorly understood.

Understanding the effects of disorder on quantum transport of massless Dirac fermions is also a challenging but fundamental task. For a single scattering event, the spin (or pseudospin for graphene) quantum degree of freedom may lead to partial or full suppression of backward reflection when the charge crosses a local tunneling barrier (referred to as the Klein tunneling mechanism [20–22]). Additionally, quantum interferences between propagating trajectories may lead to an increase of the semiclassical conductivity monitored by the π Berry phase (weak antilocalization) [23–25]. These mechanisms prevent the transition to a strong Anderson localization regime and vanishing conductivity; their dependence on the nature and strength of disorder demands in-depth scrutiny.

All types of nonmagnetic disorders, including structural imperfections (e.g., vacancies), surface contaminants, or doping with chemical impurities [26–29], preserve time-reversal symmetry and are expected to weakly affect TI transport physics. In contrast, magnetic impurities can develop net magnetic moments inducing local magnetic ordering, spin-dependent scattering, or gap formation [30–35]. Henk and co-workers [36] recently reported on the robustness of Dirac states upon moderate Mn doping of a Bi_2Te_3 surface layer. However, they observed complicated spin textures for both undoped as well as Mn-doped Bi_2Te_3, which exhibited layer-dependent spin reversal and spin vortices. Since the topological protection of Dirac states is inherently driven by the nontrivial topology of bulk electronic wave functions, surface and bulk disorders are actually expected to tailor spin polarization features. However, these effects and their relation to the Anderson localization of Dirac fermions have yet to be quantified.

This Letter describes 3D models of TI thin films and show that Dirac-cone characteristics on opposite surfaces

of the film can be tuned upon differentiation of atomic-scale surface terminations. Reducing the film thickness to several bulk layers leads to a loss of low-energy Dirac physics, owing to quantum tunneling between chiral states lying at opposite surfaces. In striking contrast, when atomic-scale bottom and top surfaces are geometrically differentiated, Dirac cones develop either at the Γ point (single Dirac cone) or at M points (three Dirac cones) and remain uncoupled down to a few bulk layers. Furthermore, upon analyzing the spin textures of Dirac states on surfaces of thick TI films as a function of the strength of nonmagnetic bulk disorder, we found that disorder leads to steady randomization of polarization properties and to suppression of certain spin-momentum-locking symmetries.

Model.—To describe the 3D-TI films, we used the Fu-Kane-Mele Hamiltonian, which is defined on a diamond lattice with a single orbital per site [37]. This is a three-dimensional generalization of the model proposed by Kane and Mele to study the quantum spin Hall effect in two-dimensional honeycomb lattices in the presence of spin-orbit coupling [1,38]:

$$\mathcal{H} = t\sum_{\langle ij\rangle} c_i^\dagger c_j + i(8\lambda_{\mathrm{SO}}/a^2)\sum_{\langle\langle ij\rangle\rangle} c_i^\dagger \mathbf{s}\cdot(\mathbf{d}_{ij}^1 \times \mathbf{d}_{ij}^2)c_j. \quad (1)$$

The first term denotes the hopping term ($t > 0$) between nearest neighboring orbitals, while the second describes the spin-orbit interaction given by a spin-dependent complex term connecting second neighbors i and j in the diamond structure through vectors $\mathbf{d}_{ij}^1$ and $\mathbf{d}_{ij}^2$ along first-neighbor bonds [see Fig. 1(a)]. λ_{SO} is the spin-orbit interaction strength, a is the cubic cell size, and $\mathbf{s} = (\sigma^x, \sigma^y, \sigma^z)$ is elaborated from the Pauli matrices. From the diamond bulk Hamiltonian, we create slabs with varying numbers of layers (up to 48) and (111) surface orientation.

An important feature of the Fu-Kane-Mele model is that it enables the description of either a weak or a strong topological insulator depending on the value of the hopping t' along the (111) direction [see Fig. 1(c)]. When $t' < t$, a weak topological insulating phase is generated whose physics resembles that of stacked bilayer bismuth, where each layer is in a 2D quantum spin Hall state [39]. This phase is characterized by an even number of Dirac points in the surface Brillouin zone (SBZ). Alternatively, if $t' > t$, the system is driven into a strong topological insulating (STI) phase, with an odd number of Dirac cones centered at the M points in the SBZ. Such a phase has been found, for instance, in $Bi_{1-x}Sb_x$ [5].

Here we focus on the STI phase, which seems more relevant in light of recent experimental works [4–6,18,40–43], and show that a gap can form at the M points (by removing the outermost layers of a diamond slab) and create a new surface Dirac cone at the Γ point [9] showing a band inversion at $\mathbf{k} = 0$. This extends the applicability of the Fu-Kane-Mele model to strong topological insulators such as Bi_2Se_3, Bi_2Te_3, or Sb_2Te_3 and could enable further modeling of some ternary [44,45] and noncentrosymmetric [46] compounds.

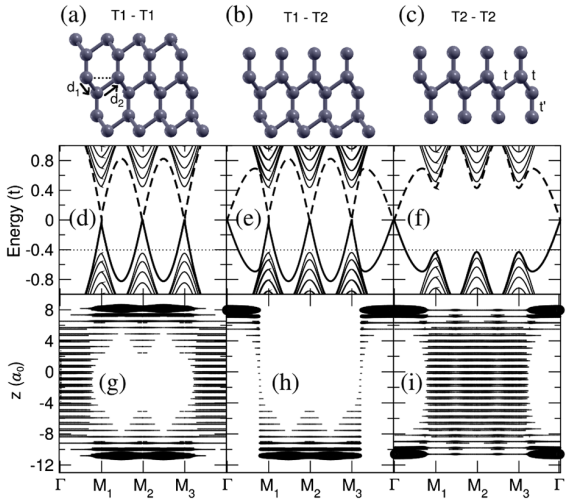

FIG. 1 (color online). (a)–(c) Thin slabs showing the atomic structure of the top and bottom surfaces for the $T1$-$T1$, $T1$-$T2$, and $T2$-$T2$ slab geometries. (d)–(f) Band structure along the path Γ-M_1-M_2-M_3-Γ for the three slab geometries shown in (a)–(c). In the $T1$-$T2$ case, the bands are no longer degenerated due to inversion symmetry breaking. (g)–(i) Charge density plots corresponding to the degenerate valence bands $|\Psi_{\mathrm{VB}}(\mathbf{k})|^2$ and $|\Psi'_{\mathrm{VB}}(\mathbf{k})|^2$ obtained for each slab geometry.

Dirac cone engineering by atomic-scale surface geometry differentiation.—Figures 1(d)–1(f) show the band structures of the three different diamond films obtained by varying surface terminations. We have fixed $t = 1$, $t' = 1.4$, and $\lambda_{\mathrm{SO}} = 1/8$ and have used a unit cell with $N = 48$ sites (one site per layer) which corresponds to a slab thickness of about $19a_0$ (where $a_0 = a/\sqrt{2}$ is the distance between second-neighbor atoms in the diamond lattice). The slab with standard termination in both surfaces [see Fig. 1(a)] has already been investigated by Fu and co-workers in Ref. [37]. We label this termination $T1$ and the related slab geometry $T1$-$T1$. The band structure for this $T1$-$T1$ geometry shows three Dirac cones located at the three equivalent M points in the SBZ [Fig. 1(d)]. Since this geometry preserves inversion symmetry, all the bands are twofold degenerated with three Dirac cones located on each surface as shown by the charge density plot corresponding to the degenerate valence bands $|\Psi_{\mathrm{VB}}(\mathbf{k})|^2$ and $|\Psi'_{\mathrm{VB}}(\mathbf{k})|^2$ [Fig. 1(g)], calculated along the path Γ-M_1-M_2-M_3-Γ.

Removing the uppermost layer from the top surface (while keeping the second-neighbor hopping within the layer underneath), one generates another termination labeled $T2$ [see Fig. 1(b)]. The corresponding slab geometry with differing terminations is labeled $T1$-$T2$, and its band structure exhibits four Dirac cones along the path Γ-M_1-M_2-M_3-Γ [Fig. 1(e)]. Although the number of Dirac cones is even, the system remains in the STI phase, because the number of Dirac points on each surface remains odd. In fact, the three Dirac cones located at the M points are related to the surface with $T1$ termination, while the single

Dirac cone (emerging at the Γ point) is localized at the $T2$ terminated surface, as evidenced by the valence band charge density plot [Fig. 1(h)]. In such a $T1$-$T2$ slab geometry, the inversion symmetry is broken, and the valence and conduction bands are no longer degenerated. However, the topological states in both surfaces can be continuously transformed from one to another by tuning the wave vector. This fact has important implications regarding film thickness, as we explain below. A third possible structure is obtained by also removing one layer from the bottom surface, which leads to a $T2$-$T2$ slab geometry [Fig. 1(c)]. The electronic structure of this slab includes a single Dirac cone at the Γ point in the SBZ of each surface [Fig. 1(f)] and resembles the typical band structure of topological insulators like Bi_2Se_2 [6] or Bi_2Te_3 [40]. The valence band charge density plot shows that the states at the Dirac cones are localized at opposite surfaces [Fig. 1(i)].

We now compute the spin texture on each surface for the three slab geometries by evaluating the expectation value of the spin operator $\langle \hat{\mathbf{s}} \rangle$ of the corresponding surface valence band state $\Psi_{\mathrm{VB}}(\mathbf{k})$ projected onto the surface sites i (with τ, τ' being the spin indices):

$$\mathbf{S}(\mathbf{k}) = \sum_{\substack{i \in \mathrm{surf} \\ \tau,\tau'}} \langle \Psi_{\mathrm{VB}}(\mathbf{k}) | i, \tau \rangle \langle i, \tau | \hat{\mathbf{s}} | i, \tau' \rangle \langle i, \tau' | \Psi_{\mathrm{VB}}(\mathbf{k}) \rangle. \quad (2)$$

In Fig. 2, we superimpose the spin textures [restricted to $E/t = -0.4 \pm 0.1$; see the dotted line in Figs. 1(d)–1(f)] on the valence band energy where Dirac points correspond to the brightest areas ($E = 0$). The top and bottom figures correspond to the top and bottom surfaces, respectively. Blue and red arrows, respectively, correspond to negative and positive z components (out of plane) of the spin. For the three studied surface terminations, the states around the Dirac points show an out-of-plane helical spin texture preserving time-reversal symmetry. It is noteworthy that in the $T1$-$T1$ and $T2$-$T2$ cases, the spin polarizations in the two surfaces are related by inversion symmetry and exhibit a vortex or a spin reversal texture. This is not the case for the $T1$-$T2$ case, in which the inversion symmetry is broken and the spin texture is centered around the Γ point (at the top surface) and the three M points (at the bottom surface).

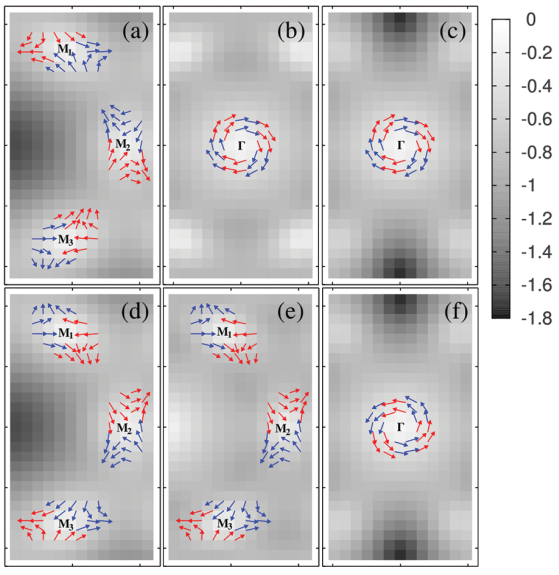

FIG. 2 (color). Spin texture on top and bottom surfaces (top and bottom panels, respectively) for the three different slabs studied (a), (d) $T1$-$T1$, (b), (e) $T1$-$T2$, and (c), (f) $T2$-$T2$. The gray scale indicates the valence band energy where the Dirac cones are located at the bright spots.

TI-film thickness and robustness of Dirac physics.—Figure 3 gives the electronic structures of slabs with varying film thickness. For the $T1$-$T1$ terminated structure, a sizable gap already opens at all M points for slabs with 12 layers. However, reducing the thickness down to four layers [Fig. 3(d)] provides insulating surface states, since gap values are above 1 (in t units). For the $T2$-$T2$ case, the twelve-layer slab evidences a small gap at Γ which is further widened upon reduction of film thickness [Figs. 3(c) and 3(f)]. Note that a similar situation has been encountered in recent experiments [18,47]. For four layers, a gap of approximately 1 (in t units) develops, similarly to the $T1$-$T1$ termination. Turning to the mixed ($T1$-$T2$) termination, one might expect a similar trend. However, the behavior is completely different [see Figs. 3(b) and 3(e)]: Gapless surface states are insensitive to quantum tunneling, and gap formation is suppressed regardless of film thickness. These results support the interpretation of recent experiments by Bian and coworkers [19], who also reported the absence of a gap opening for thin TI films. In that case, strong interfacial bonding to the substrate prevents gap opening, in contrast to freestanding TI films.

Bulk disorder effects on spin textures.—We investigate the changes in the spin texture upon introduction of bulk disorder. It is indeed very instructive to determine the extent to which the topological protection of surface states is reduced in the presence of bulk disorder with increasing strength. To facilitate comparison with experiments, we

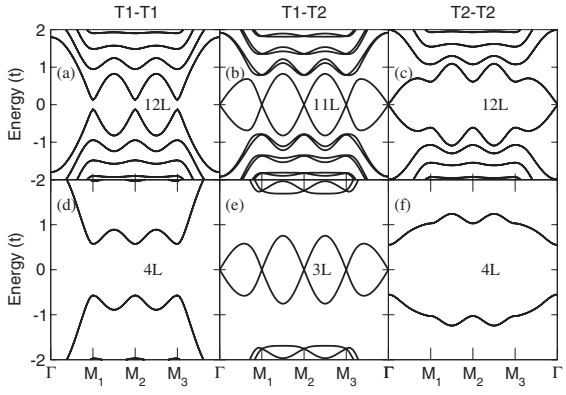

FIG. 3. Band structure of slabs of various thicknesses (layers L) and surface terminations made from the STI phase as explained in the text. The surface terminations of upper and lower surfaces are $T1$-$T1$ (a), (d), $T1$-$T2$ (b), (e), and $T2$-$T2$ (c), (f).

focus on the geometry which induces single Γ-centered Dirac points ($T2$-$T2$ surface configuration). For each k point close to Γ, the spin vectors $\mathbf{S}(\mathbf{k})$ are computed [by using Eq. (2) but neglecting surface projection] for the valence band. The spin textures are plotted for the clean case in Fig. 4(c) (semitransparent arrows), where the in-plane projection is indicated by the vector length and the out-of-plane component by the color index. For all k points in the vicinity of Γ, the total length is 1 (in units of $\hbar/2$).

The introduction of bulk disorder (excluded from surface layers) is found to alter surface spin textures [48]. To monitor these changes, we compute the total norm of the spin vectors taken from a regular grid of k points and a series of (up to 100) different disorder configurations and then plot their statistics in histograms (Fig. 4). A generic model of Anderson disorder [49] is included through a modulated potential profile (ε_i), with ε_i selected at random in the interval $[-W/2, W/2]$. This model mimics impurities or structural defects and has been widely employed in the literature for exploring metal-insulator transition [29,50,51]. We use a 12-layer-thick supercell containing 9 (i.e., 3×3) unit cells [52].

Upon varying the disorder strength W [Figs. 4(a) and 4(b)], we find that, as long as $W \leq 1$, the spin textures remain unchanged by bulk disorder, whereas starting from $W \simeq 2$, spin polarization starts being randomized with a reduced norm (for $W \geq 4$) which eventually vanishes in the strong disorder limit. An illustration of the randomization and loss of spin polarization for $W = 4$ and 9 unit cells is given in Fig. 4(c) (opaque arrows) in comparison to the clean case.

To unveil the mechanism leading to the randomization of the spin polarization, we plot the absolute square of the valence band wave function $|\Psi_{\mathrm{VB}}(\mathbf{k})|^2$ near the Γ point ($\mathbf{k} = \Gamma + \delta$) along the z axis perpendicular to the surface [Fig. 4(d)]. For $W = 0$, the valence band wave function is mainly localized at the surface, but as the disorder strength is tuned from $W = 4$ to $W = 10$, it further spreads over bulk layers. The observed penetration depth of electronic states progressively increases with W, changing the nature of wave functions from (quasi-)two-dimensional confined states at the surface to more three-dimensional real-space extended states promoted by bulk disorder [53]. For $W = 10$, the wave function is seen to be spread all over the system. However, we also observe that intersurface coupling mediated by bulk disorder is a minor effect. In fact, from a comparison of spin polarization histograms for different slab thicknesses [52], we conclude that intersurface coupling between Dirac cones is negligible for spin randomization at thicknesses down to 12 layers.

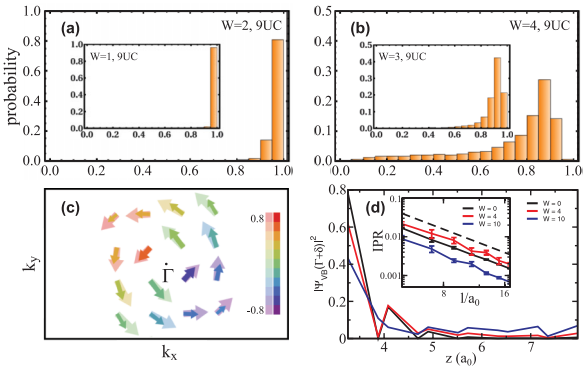

FIG. 4 (color). Spin polarization of the $T2$-$T2$ slab (12 layers) with disorder. (a), (b) Norm distribution of spin vectors close to Γ. (c) Spin texture of a clean (semitransparent) and disordered slab (opaque). (d) Squared valence band wave function near the Γ point for different disorder and IPR for increasing lateral slab size (inset). The l^{-2} scaling behavior is shown as dashed lines.

To deepen the analysis, we compute and analyze the scaling behavior of the inverse participation ratio defined as $\mathrm{IPR} = \sum_i |\Psi_{\mathrm{VB}}|^4 / ([\sum_i |\Psi_{\mathrm{VB}}|^2]^2)$. The inverse participation ratio (IPR) is a common measure for the localization nature of electronic states (see, e.g., Ref. [54]). In the absence of disorder, the IPR scales as l^{-d} (where l is system length and d the space dimension) being a fingerprint of truly extended states and a metallic regime, whereas the Anderson localization regime (in the strong disorder limit) manifests in a length-independent IPR value (with $\mathrm{IPR} \sim \xi^{-d}$, ξ the localization length). Figure 4(d) (inset) shows IPR for increasing lateral slab sizes l and for $W = 0, 4$, and 10. It is found that $\mathrm{IPR} \sim l^{-2}$ for $W = 0$, in agreement with extended wave functions at the surface [only weak unavoidable spreading to nearest bulk layers is observed for $|\Psi_{\mathrm{VB}}|^2$; Fig. 4(d) (main frame)]. By increasing the bulk disorder strength from $W = 4$ to $W = 10$, the IPR are seen to vary in absolute value in a nonmonotonic fashion while maintaining the $\mathrm{IPR}(l) \sim l^{-2}$ scaling behavior, with no sign of saturation for the considered system sizes. This scaling analysis excludes short localization lengths and the Anderson insulating regime for bulk disorder strengths, which, however, significantly suppress surface spin polarization.

Conclusion.—Engineering of Dirac cones in models of 3D-TI films with varying thickness and surface termination have been reported. Absence of gap formation has been found in ultrathin TI for structurally differentiated surfaces, a feature in agreement with recent works [19]. Bulk disorder was found to yield randomization of surface spin polarization driven by the penetration of boundary states inside the film. These findings (of relevance for Bi_2Se_3 and related TI) suggest an analysis of bulk crystalline quality of TI by inspecting the spin texture at ultraclean TI surfaces, in a regime far from the Anderson insulating regime.

D. S. and F. O. contributed equally to this work. The author thankfully acknowledge computer resources, technical expertise and assistance provided by the Barcelona Supercomputing Center—Centro Nacional de Supercomputación, the Spanish Supercomputing Network and the BIFI—University of Zaragoza.

[1] C. L. Kane and E. J. Mele, Phys. Rev. Lett. **95**, 226801 (2005).
[2] A. Bernevig, T. L. Hughes, and S.-C. Zhang, Science **314**, 1757 (2006).
[3] M. König, S. Wiedmann, C. Brüne, A. Roth, H. Buhmann, L. W. Molenkamp, X.-L. Qi, and S.-C. Zhang, Science **318**, 766 (2007).
[4] D. Hsieh, D. Qian, L. Wray, Y. Xia, Y. S. Hor, R. J. Cava, and M. Z. Hasan, Nature (London) **452**, 970 (2008).
[5] D. Hsieh, Y. Xia, L. Wray, D. Qian, A. Pal, J. H. Dil, J. Osterwalder, F. Meier, G. Bihlmayer, C. L. Kane, Y. S. Hor, R. J. Cava, and M. Z. Hasan, Science **323**, 919 (2009).
[6] Y. Xia, D. Qian, D. Hsieh, L. Wray, A. Pal, H. Lin, A. Bansil, D. Grauer, Y. S. Hor, R. J. Cava, and M. Z. Hasan, Nat. Phys. **5**, 398 (2009).
[7] H. Zhang, C.-X. Liu, X.-L. Qi, X. Dai, Z. Fang, and S.-C. Zhang, Nat. Phys. **5**, 438 (2009).
[8] O. V. Yazyev, J. E. Moore, and S. G. Louie, Phys. Rev. Lett. **105**, 266806 (2010).
[9] M. Z. Hasan and C. L. Kane, Rev. Mod. Phys. **82**, 3045 (2010).
[10] M. Z. Hasan and J. E. Moore, Annu. Rev. Condens. Matter Phys. **2**, 55 (2011).
[11] X.-L. Qi and S.-C. Zhang, Rev. Mod. Phys. **83**, 1057 (2011).
[12] P. Cheng, C. Song, T. Zhang, Y. Zhang, Y. Wang, J.-F. Jia, J. Wang, Y. Wang, B.-F. Zhu, X. Chen, X. Ma, K. He, L. Wang, X. Dai, Z. Fang, X. Xie, X.-L. Qi, C.-X. Liu, S.-C. Zhang, and Q.-K. Xue, Phys. Rev. Lett. **105**, 076801 (2010).
[13] T. Hanaguri, K. Igarashi, M. Kawamura, H. Takagi, and T. Sasagawa, Phys. Rev. B **82**, 081305(R) (2010).
[14] C.-X. Liu, X.-L. Qi, and S.-C. Zhang, Physica (Amsterdam) **44E**, 906 (2012).
[15] S. Kim, M. Ye, K. Kuroda, Y. Yamada, E. E. Krasovskii, E. V. Chulkov, K. Miyamoto, M. Nakatake, T. Okuda, Y. Ueda, K. Shimada, H. Namatame, M. Taniguchi, and A. Kimura, Phys. Rev. Lett. **107**, 056803 (2011).
[16] H. Steinberg, J.-B. Laloë, V. Fatemi, J. S. Moodera, and P. Jarillo-Herrero, Phys. Rev. B **84**, 233101 (2011).
[17] A. H. Castro-Neto, F. Guinea, N. Peres, K. Novoselov, and A. Geim, Rev. Mod. Phys. **81**, 109 (2009).
[18] A. A. Taskin, S. Sasaki, K. Segawa, and Y. Ando, Phys. Rev. Lett. **109**, 066803 (2012).
[19] G. Bian, X. Wang, Y. Liu, T. Miller, and T.-C. Chiang, Phys. Rev. Lett. **108**, 176401 (2012).
[20] T. Ando, T. Nakanishi, and R. Saito, J. Phys. Soc. Jpn. **67**, 2857 (1998).
[21] M. Katsnelson, K. Novoselov, and A. Geim, Nat. Phys. **2**, 620 (2006).
[22] J. Moore, Nature (London) **464**, 194 (2010).
[23] E. McCann, K. Kechedzhi, V. I. Falko, H. Suzuura, T. Ando, and B. L. Altshuler, Phys. Rev. Lett. **97**, 146805 (2006).
[24] H.-Z. Lu, J. Shi, and S.-Q. Shen, Phys. Rev. Lett. **107**, 076801 (2011).
[25] H.-Z. Lu and S.-Q. Shen, Phys. Rev. B **84**, 125138 (2011).
[26] H.-J. Noh, J. Jeong, E.-J. Cho, H.-K. Lee, and H.-D. Kim, Europhys. Lett. **96**, 47002 (2011).
[27] W.-Y. Shan, J. Lu, H.-Z. Lu, and S.-Q. Shen, Phys. Rev. B **84**, 035307 (2011).
[28] A. M. Black-Schaffer and A. V. Balatsky, Phys. Rev. B **85**, 121103(R) (2012).
[29] G. Schubert, H. Fehske, L. Fritz, and M. Vojta, Phys. Rev. B **85**, 201105(R) (2012).
[30] D. Culcer, Physica (Amsterdam) **44E**, 860 (2012).
[31] S. Caprara, V. V. Tugushev, P. M. Echenique, and E. V. Chulkov, Phys. Rev. B **85**, 121304 (2012).
[32] G. Rosenberg and M. Franz, Phys. Rev. B **85**, 195119 (2012).
[33] M. S. Foster, Phys. Rev. B **85**, 085122 (2012).
[34] J. Honolka, A. A. Khajetoorians, V. Sessi, T. O. Wehling, S. Stepanow, J.-L. Mi, B. B. Iversen, T. Schlenk, J. Wiebe, N. Brookes, A. I. Lichtenstein, P. Hofmann, K. Kern, and R. Wiesendanger, Phys. Rev. Lett. **108**, 256811 (2012).
[35] M. Ye, S. V. Eremeev, K. Kuroda, E. E. Krasovskii, E. V. Chulkov, Y. Takeda, Y. Saitoh, K. Okamoto, S. Y. Zhu, K. Miyamoto, M. Arita, M. Nakatake, T. Okuda, Y. Ueda, K. Shimada, H. Namatame, M. Taniguchi, and A. Kimura, Phys. Rev. B **85**, 205317 (2012).
[36] J. Henk, A. Ernst, S. V. Eremeev, E. V. Chulkov, I. V. Maznichenko, and I. Mertig, Phys. Rev. Lett. **108**, 206801 (2012).
[37] L. Fu, C. L. Kane, and E. J. Mele, Phys. Rev. Lett. **98**, 106803 (2007).
[38] C. L. Kane and E. J. Mele, Phys. Rev. Lett. **95**, 146802 (2005).
[39] S. Murakami, Phys. Rev. Lett. **97**, 236805 (2006).
[40] Y. L. Chen, J. G. Analytis, J.-H. Chu, Z. K. Liu, S.-K. Mo, X. L. Qi, H. J. Zhang, D. H. Lu, X. Dai, Z. Fang, S. C. Zhang, I. R. Fisher, Z. Hussain, and Z.-X. Shen, Science **325**, 178 (2009).
[41] S. Y. Xu, Y. Xia, L. A. Wray, S. Jia, F. Meier, J. H. Dil, J. Osterwalder, B. Slomski, A. Bansil, H. Lin, R. J. Cava, and M. Z. Hasan, Science **332**, 560 (2011).
[42] H. Beidenkopf, P. Roushan, J. Seo, L. Gorman, I. Drozdov, Y. S. Hor, R. J. Cava, and A. Yazdani, Nat. Phys. **7**, 939 (2011).
[43] T. Valla, Z.-H. Pan, D. Gardner, Y. S. Lee, and S. Chu, Phys. Rev. Lett. **108**, 117601 (2012).
[44] H.-J. Zhang, S. Chadov, L. Müchler, B. Yan, X.-L. Qi, J. Kübler, S.-C. Zhang, and C. Felser, Phys. Rev. Lett. **106**, 156402 (2011).
[45] X.-Q. Dai, B. Zhao, J.-H. Zhao, Y.-H. Li, Y.-N. Tang, and N. Li, J. Phys. Condens. Matter **24**, 035502 (2012).
[46] M. S. Bahramy, B. J. Yang, R. Arita, and N. Nagaosa, Nat. Commun. **3**, 679 (2012).
[47] Y. Zhang, C.-Z. Chang, C.-L. Song, L.-L. Wang, X. Chen, J.-F. Jia, Z. Fang, X. Dai, W.-Y. Shan, S.-Q. Shen, Q. Niu, X.-L. Qi, S.-C. Zhang, X.-C. Ma, and Q.-K. Xue, Nat. Phys. **6**, 584 (2010).
[48] A. Kundu, A. Zazunov, A. Levy Yeyati, T. Martin, and R. Egger, Phys. Rev. B **83**, 125429 (2011).
[49] P. W. Anderson, Phys. Rev. **109**, 1492 (1958).
[50] P. A. Lee and D. S. Fisher, Phys. Rev. Lett. **47**, 882 (1981).
[51] F. Evers and A. D. Mirlin, Rev. Mod. Phys. **80**, 1355 (2008).
[52] See Supplemental Material at http://link.aps.org/supplemental/10.1103/PhysRevLett.109.266805 for further spin distributions and penetration depths for different supercells.
[53] J. Linder, T. Yokoyama, and A. Sudbo, Phys. Rev. B **80**, 205401 (2009).
[54] J. Brndiar and P. Markos, Phys. Rev. B **77**, 115131 (2008).